Supporting Information for

Enhancement of ionic conductivity of a composite polymer electrolyte via surface functionalization of SSZ-13 zeolite for all-solid-state Li-ion batteries

Hasan Jamal[a], Firoz Khan[b], Suyeon Hyun[a], Sang Won Min[a] and Jae Hyun Kim[a]

[a]Division of Energy Technology, Daegu Gyeongbuk Institute of Science & Technology, 333, Techno Jungang-Daero, Hyeonpung-Myeon, Dalseong-Gun, Daegu 42988,

Republic of Korea

[b]Center of Research Excellence in Renewable Energy (CORE-RE), King Fahd University of Petroleum & Minerals (KFUPM), Dhahran 31261, Saudi Arabia

*Correspondence: jaehyun@dgist.ac.kr; Tel.: +82-53-7853-610; Fax: +82-53-7853-439

Synthesis of LFP and NCA cathodes

The charge-discharge measurements of CPEs were conducted using the CR2032 type coin cell structure. The cathode was realized using LFP, while the Li-foil was acted as an anode. The cathode slurry was composed of 90 wt.% LFP powder, 5 wt.% super P, and 5 wt.% polyvinylidene fluoride (PVDF). The constituents of the cathode were dissolved in N-Methyl-2-pyrrolidone (NMP) using high energy ball-milling mixing. Then coated on the Al-foil and dried in vacuum at 110 ℃ for 12 h. The charge-discharged analysis was done using an instrument (WonATech, WBCS3000) between 2.6 V–4.3 V at a current density of 0.1 C. The specific capacity was calculated through the mass of active material. The current density at 1C = 170 mA/g for the LFP cathode. The area mass loading of the active material was 2.2 mg/cm^2. A similar cathode fabrication process was used for NCA with the same mass loading. The current density at 1C = 195 mA/g for the NCA cathode.

Fabrication of coin cells for charge/discharge measurements

The coin cells were fabricated using three types of solid electrolytes i.e., SPE, 5% CPE, and 5% MZ-CPE. The Li-foil is used as an anode for all the cells. LFP was used as a cathode for SPE and 5% CPE solid electrolytes, whereas two types of cathodes were used for 5% MZ-CPE solid electrolyte. Thus, the cell structures for SPE and 5% CPE solid electrolytes were [Li|SPE|LFP] and [Li|5% CPE|LFP], respectively. However, the cell structures used for 5% MZ-CPE were [Li|5% MZ-CPE|LFP] and [Li|5% MZ-CPE|NCA].

Fabrication of coin cells using liquid electrolyte for charge/discharge measurements

The coin cell structure used for liquid electrolytes was [Li|Liquid electrolytes|LFP]. 1 M LiPF6 in a mixture of ethylene carbonate–dimethyl carbonate (EC–DMC) with a volume ratio of 3: 7 was used as the liquid electrolyte (Starlyte, Korea). The Celgard 2400 membrane was used as a separator.

Degree of crystallinity calculation from DSC data

DSC data for phase transition behavior of the PEO, SPE and MZ-CPE with different content of M-SSZ-13 zeolite including glass transition temperature (T_g), Melting temperature (T_m), enthalpy of melting (ΔH_m) and degree of crystallinity (X_c).

$$x_C \equiv \frac{\Delta H_m}{\Delta H_0} \tag{S1}$$

The degree of crystallinity (X_c) can be estimated according to Eq. (S1), where, ΔH_m was obtained from DSC results, and ΔH_0 is the melting enthalpy of 100 % crystalline PEO (213.7 J/g) reported in literature [1,2].

Activation energy calculation

The Vogel-Tamman-Fulcher (VTF) equation (S2) is used to determine the value of activation energy (E_a) of the SPE and MZ-CPEs [3].

$$\sigma = AT^{-1/2} e^{\frac{-E_a}{R(T-T_0)}} \tag{S2}$$

Where, A = pre-exponential factor, T = temperature, R = Universal gas constant (0.008314 kJ/mol/K) and T_0 = equilibrium glass-transition temperature of the copolymer (T_g -50).

The eq. (S2) can be rewritten as

$$log\left(\sigma.T^{1/2}\right) = \log(A) - \frac{E_a}{R(T-T_0)} \tag{S3}$$

The curves between $log\left(\sigma.T^{1/2}\right)$ vs. $\frac{1}{(T-T_0)}$ were plotted for each sample as shown in Fig. S18.

Furthermore, those curves were linearly fitted. The slope of the curve with the $\frac{1}{(T-T_0)}$ axis provides the value of E_a, whereas, the intercept on the $log\left(\sigma.T^{1/2}\right)$ axis gives the value of A. The obtained values of E_a and log(A) are listed in Table S5.

Table S1. Composition of SPE, Li-salt, and MZ-SSZ-13 dissolved in ACN (15 mL) for synthesis of MZ-CPE. Ball milling time for all the samples are 48 h.

Sample names	PEO (g)	LiTFSI (g)	MZ-SSZ-13 (g)
SPE	0.40	0.102	NA
5% MZ-CPE	0.40	0.102	0.0251
10% MZ-CPE	0.40	0.102	0.0502
15% MZ-CPE	0.40	0.102	0.0753
20% MZ-CPE	0.40	0.102	0.1004

Table S2. Ionic conductivities of, 5% MZ-CPE @30 ℃ With different ball-milling time.

Ball-milling duration (h)	**σ (S/cm) at 30 ℃**
48	6.16×10^{-4}
96	1.40×10^{-4}
144	1.29×10^{-4}
192	Very fragile

Table S3. DSC data for phase transition behavior of the PEO, SPE and MZ-CPE with different content of M-SSZ-13 zeolite including glass transition temperature (T_g), Melting temperature (T_m), enthalpy of melting (ΔH_m) and degree of crystallinity (X_c).

Sample names	T_g (℃)	T_m (℃)	ΔH_m (J/g)	X_c (%)
PEO	NA	70.9	176.3	82.4
SPE	-33.6	63.7	69.8	32.7
5% MZ-CPE	-36.8	60.6	67.7	31.6
10% MZ-CPE	-34.2	61.8	64.9	30.4
15% MZ-CPE	-34.8	60.2	54.9	25.7
20% MZ-CPE	-36.2	59.5	51.9	24.3

Table S4. Ionic conductivities of SPE, 5% MZ-CPE, 10% MZ-CPE, 15% MZ-CPE and 20% MZ-CPE measured at various temperatures (20, 30, 40, 50, 60 and 70 ℃).

Samples	σ (S/cm)					
	20 ℃	**30 ℃**	**40 ℃**	**50 ℃**	**60 ℃**	**70 ℃**
SPE	2.29×10^{-6}	1.84×10^{-5}	1.15×10^{-4}	5.24×10^{-4}	1.58×10^{-3}	2.34×10^{-3}
5% MZ-CPE	8.00×10^{-5}	6.16×10^{-4}	3.44×10^{-3}	1.66×10^{-2}	3.61×10^{-2}	5.34×10^{-2}
10% MZ-CPE	3.76×10^{-5}	2.16×10^{-4}	7.76×10^{-4}	6.16×10^{-3}	6.74×10^{-3}	2.45×10^{-2}
15% MZ-CPE	2.49×10^{-5}	1.38×10^{-4}	1.02×10^{-3}	3.29×10^{-3}	1.70×10^{-2}	2.39×10^{-2}
20% MZ-CPE	1.17×10^{-5}	6.60×10^{-5}	5.60×10^{-4}	2.71×10^{-3}	6.16×10^{-3}	1.20×10^{-2}

Table S5. The fitting parameter to obtain the activation energy of the polymer-based solid electrolyte.

Sample	Slop [E_a/R] (K)	Intercept [log(A)]	E_a (kJ/mol)
SPE	-873.21	4.5267	7.25987
5% MZ-CPE	-560.28	3.5953	4.65817
10% MZ-CPE	-619.11	3.5753	5.14728
15% MZ-CPE	-641.66	3.7442	5.33476
20% MZ-CPE	-700.36	3.8388	5.82279

Table S6. Measured parameter values used for the determination of t_{Li^+} at 60 ^{0}C.

Sample	I_0 (μA)	I_s (μA)	R_0 (Ω)	R_s (Ω)	ΔV (mV)	t_{Li^+}
SPE	490	1.07	264	890	5	0.29
5% CPE	566	1.25	890	1544	5	0.57
5% MZ-CPE	696	10.38	947	1120	5	0.85

Table S7. Comparison of battery performance for composite polymer electrolytes for Li-metal solid-state batteries.

Electrolyte	σ (S/cm)	Cathode/Anode	WV (V)	WT (℃)	SC (mAh/g)	TSC (mA/g)	SLR (AM:CB:BD)	RR (%) (after cycles)	LW (mg/cm^2)	Ref.
PEO-LiTFSI-MIL-53(Al)	3.9×10^{-4} @75 ℃	PANI@C/S-280/Li	1.0-3.0	80	905*	1672	80:10:10	96.7 (60)	NA	[4]
PEO-LiTFSI-HMOP	4.0×10^{-4} @65 ℃	$LiFPO_4$/Li	2.9-3.8	65	131	NA	60:10:30	91.6 (100)	2	[5]
PEO-$LiClO_4$-SiO_2	1.2×10^{-3} @60 ℃	$LiFPO_4$/Li	2.5-4.1	90	131	170	65:15:20	80 (80)	1.0	[6]
PEO-LLZTO	4.5×10^{-4} @60 ℃	$LiFPO_4$/Li	2.4-4.2	60	116	170	80:10:10	90 (200)	NA	[7]
PEO-LiTFSI-IL@ZrO_2	4.9×10^{-4} @50 ℃	N-CNs/S/Li	1.8-2.6	50	1437*	NA	70:10:20	68.6 (40)	1.18	[8]
PEO-LiTFSI-SSZ-13	4.4×10^{-5} @20 ℃ 1.91×10^{-3} @60 ℃	$LiFPO_4$/Li	2.5-4.0	58	169	NA	80:10:10	92 (160)	4.0	[9]
PEO-LiTFSI-LLZTO-SN	1.22×10^{-4} @30 ℃	$LiFPO_4$/Li	2.8-4.0	60	152	150	70:10:10	95 (50)	NA	[10]
PEO-LiPCSI	8.32×10^{-5} @65 ℃	$LiFPO_4$/Li	NA	60	141	NA	NA	85 (80)	NA	[11]
PEO-LiTFSI-M-SSZ-13	6.16×10^{-4} @30 ℃ 5.34×10^{-2} @ 70 ℃	$LiFPO_4$/Li	2.6-4.3	60	154	170	90:05:05	94.0 (80)	2.2	This work

*Lithium-Sulphur battery

WV = working voltage, WT = working temperature, SC = specific capacity, TSC = Theoretical specific capacity, RR = retention rate, LW = loading weight, SLR = slurry ratio, AM = active materials, CB = carbon black, and BD = binder

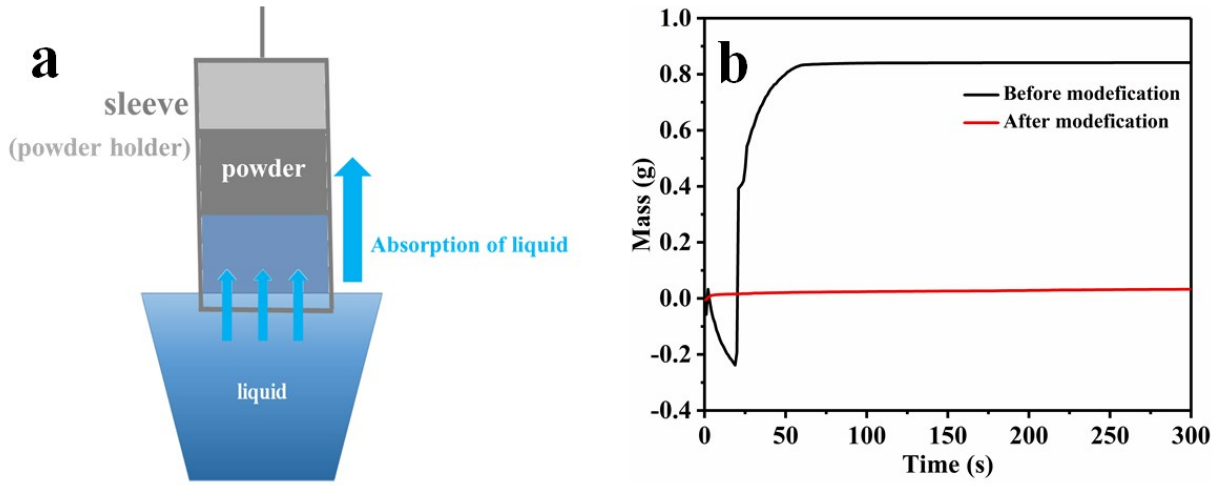

Fig. S1. (a) The schematic diagram of wettability analyser using force tensiometer and (b) the mass vs time curve for the zeolite before and after surface modification with BYK-SILCLEAN 3700.

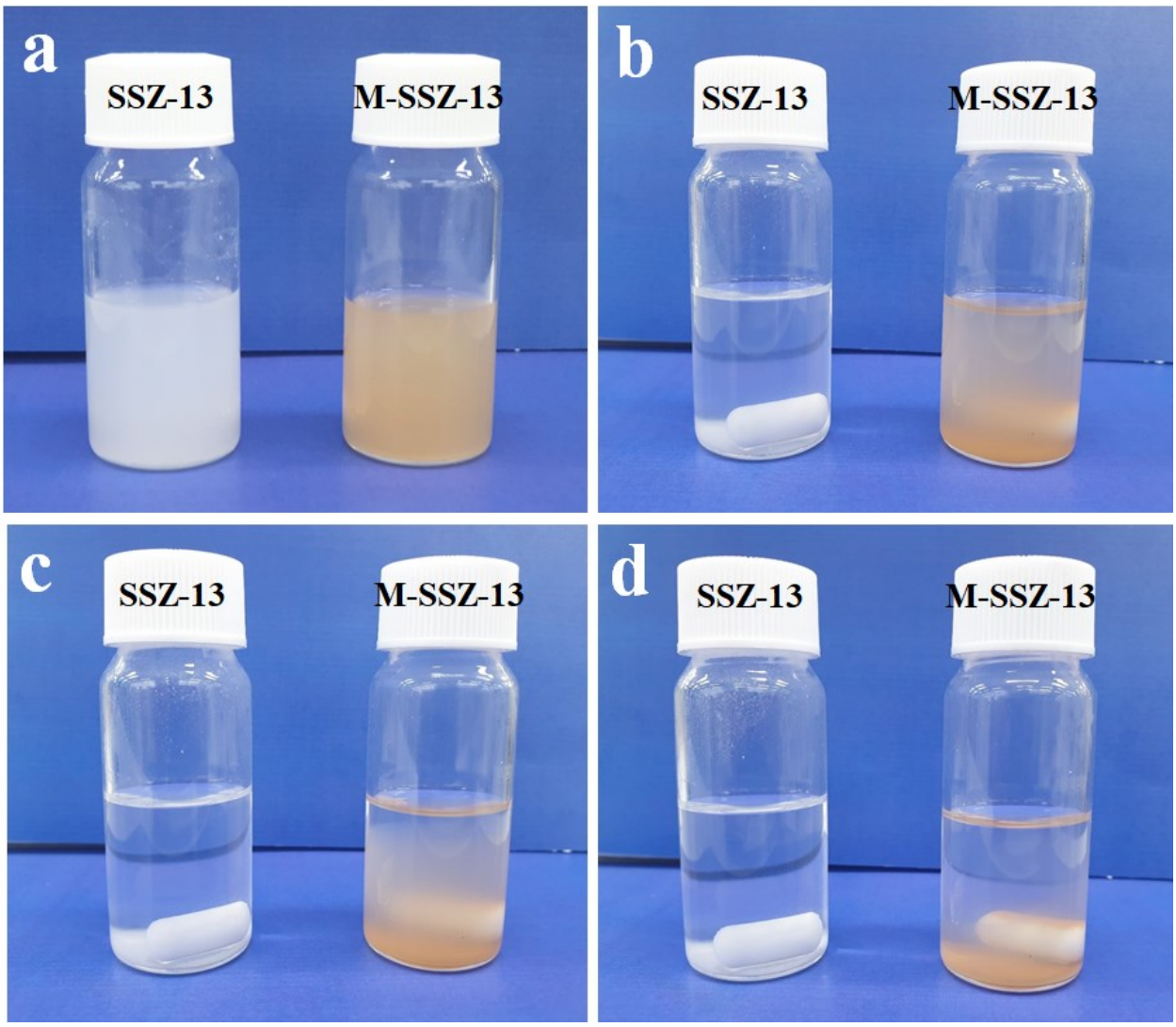

Fig. S2. Dispersion of SSZ-13 zeolite and M-SSZ-13 in ACN, (a) Right after 24 h stirring, (b) dispersion stability after 15 min, (c) dispersion stability after 1 h, and (d) dispersion stability after 3 h.

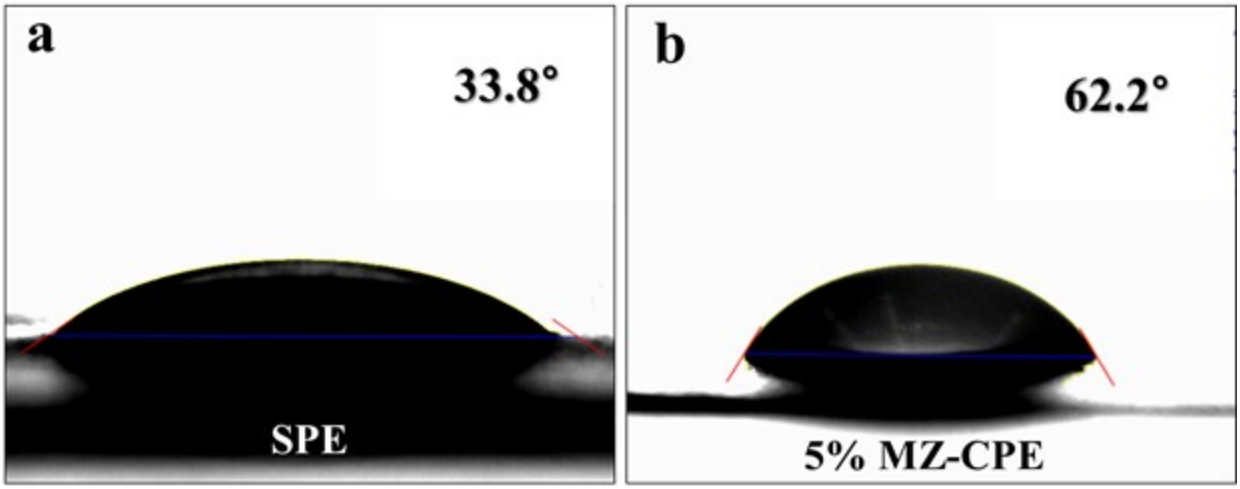

Fig. S3. Contact angle images of (a) SPE and (b) 5% MZ-CPE using deionized water droplet.

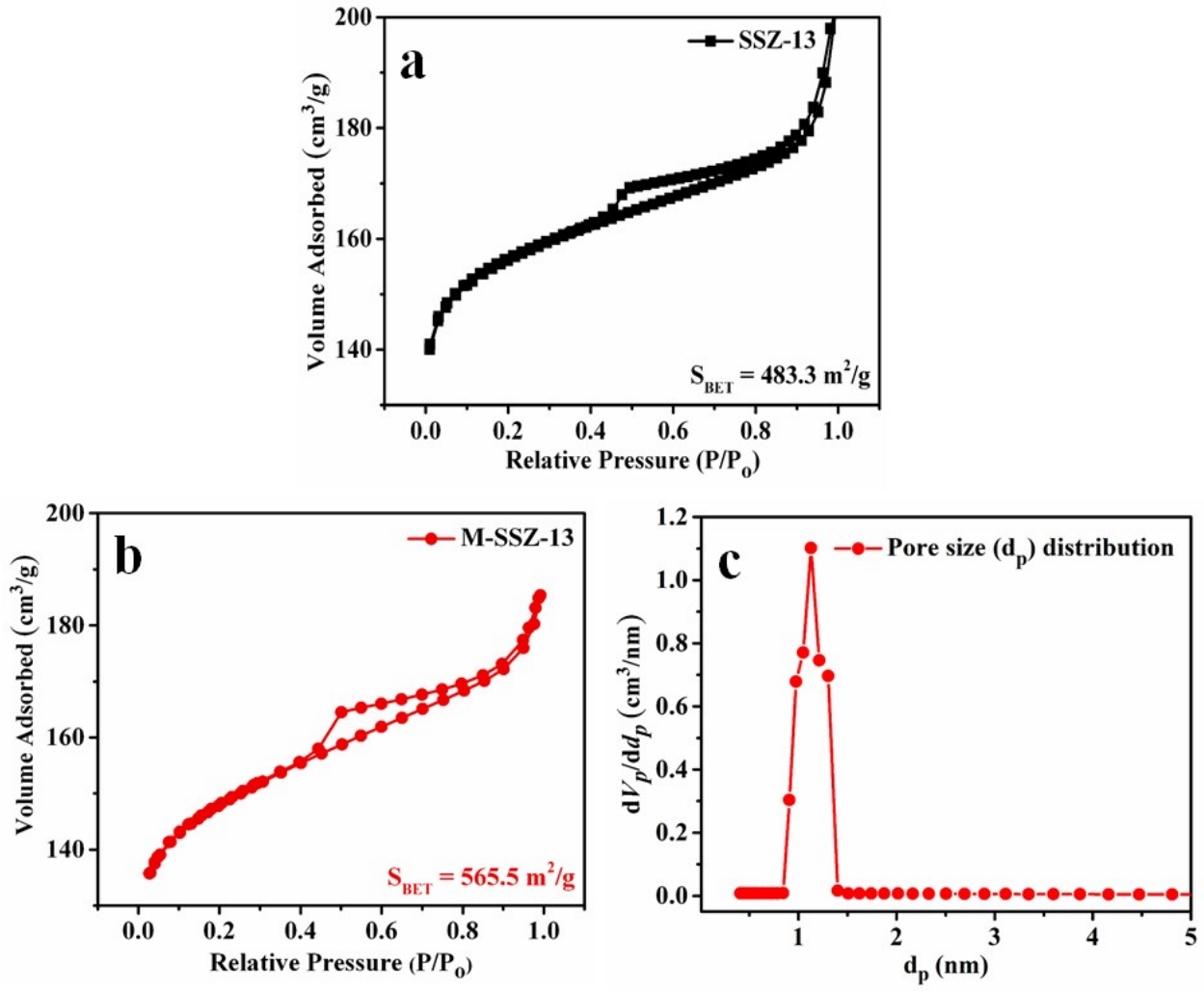

Fig. S4. Nitrogen adsorption-desorption isotherm of (a) SSZ-13 zeolite, (b) M-SSZ-13 zeolite and (c) BJH pore size (d_p) distribution curve of M-SSZ-13 Zeolite.

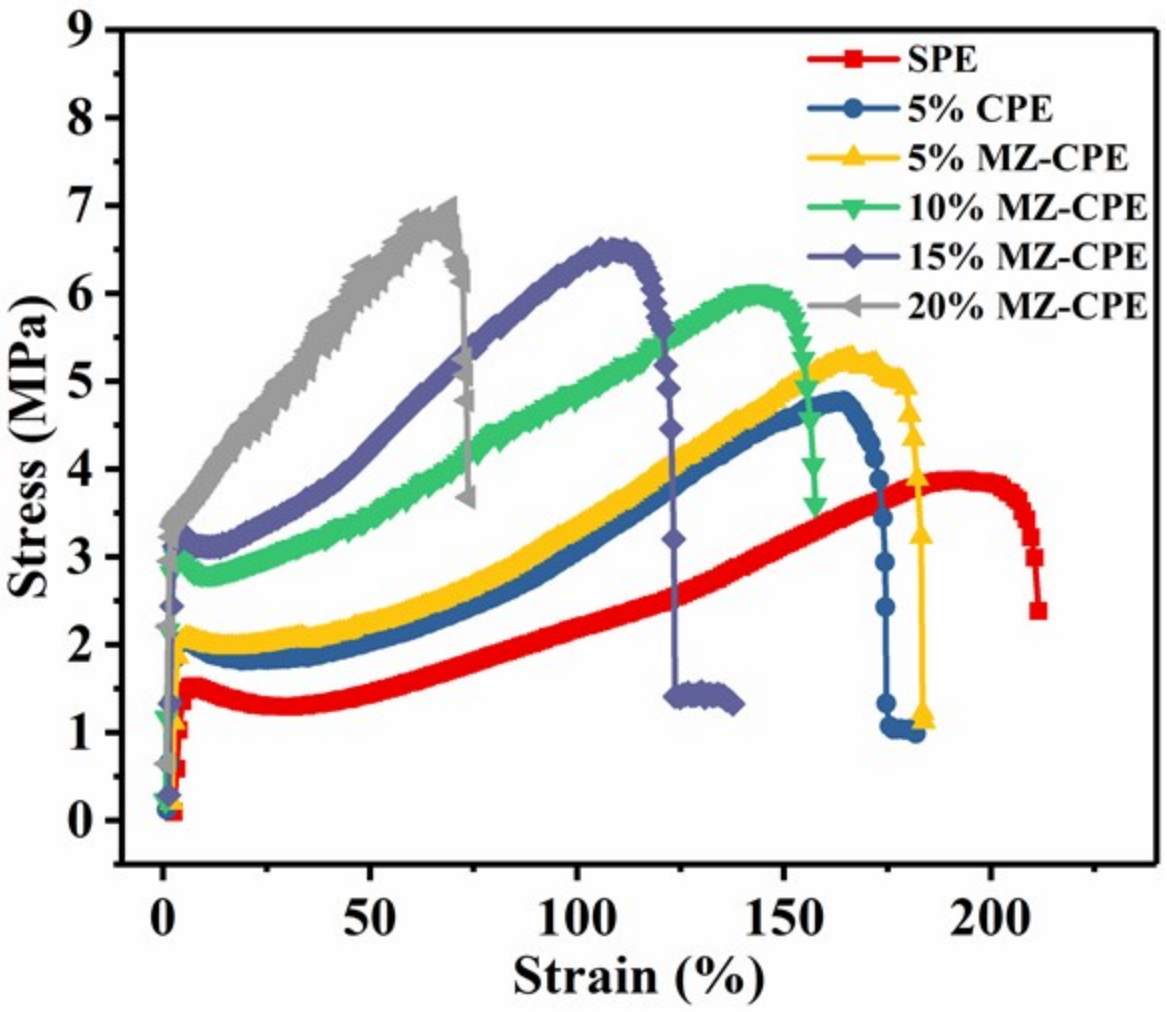

Fig. S5. Stress-strain curves of SPE, 5% CPE, 5% MZ-CPE, 10% MZ-CPE, 15% MZ-CPE, and 20% MZ-CPE solid electrolytes.

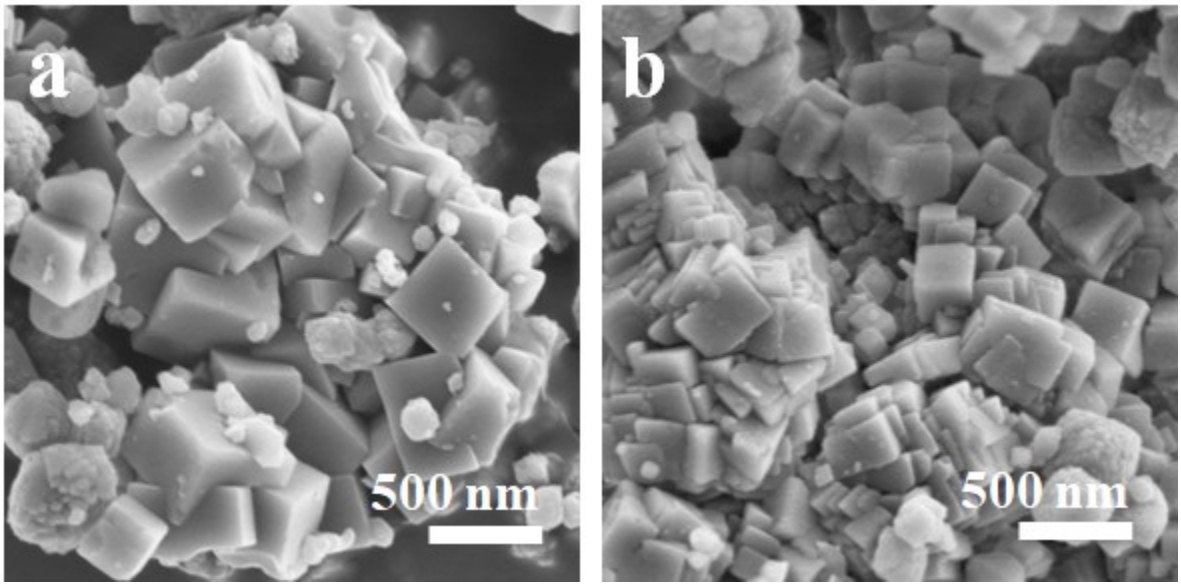

Fig. S6. FE-SEM images of (a) SSZ-13 and (b) M-SSZ-13 zeolites.

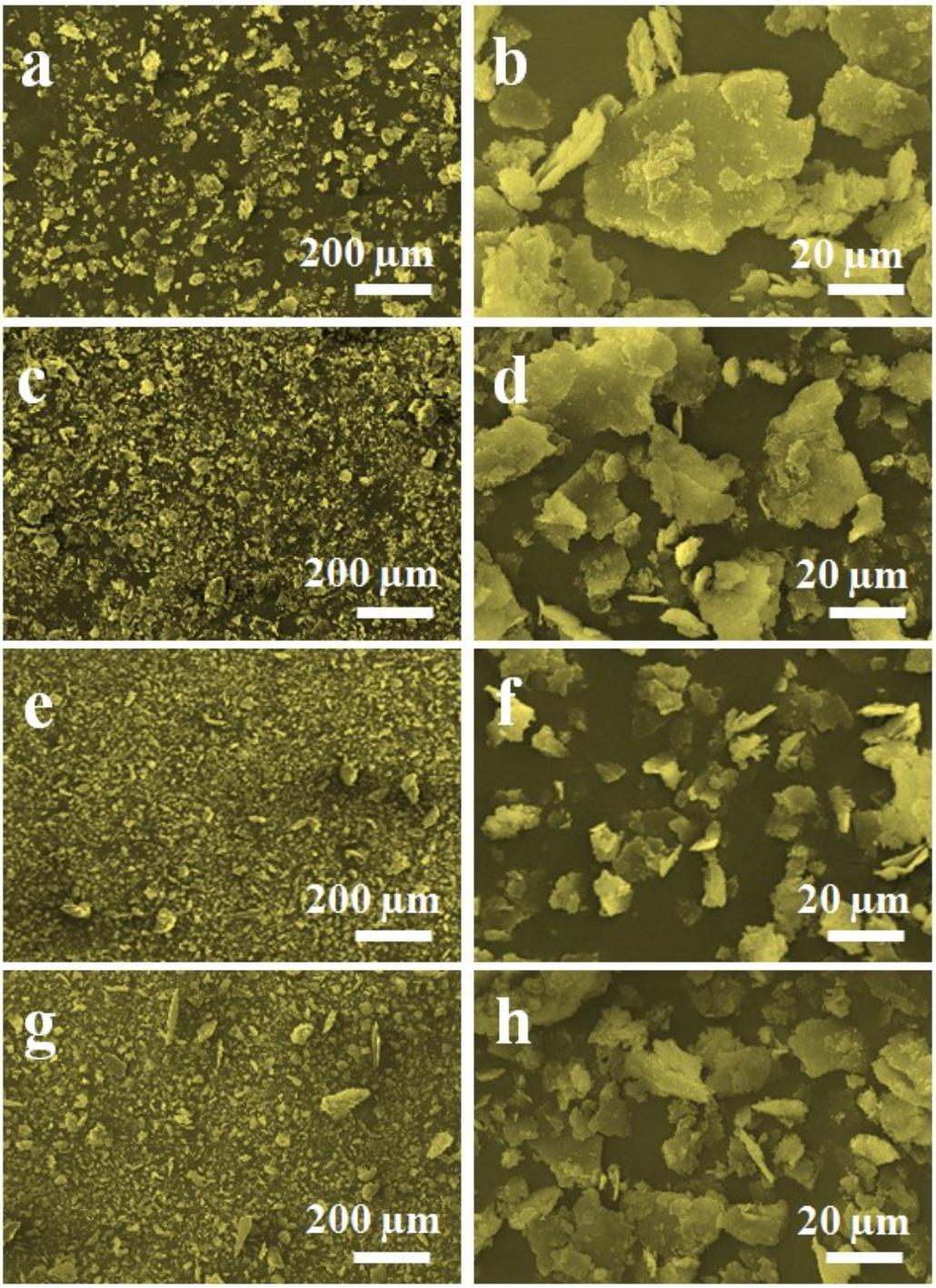

Fig. S7. SEM images of M-SSZ-13 with ACN ball-milled for various time duration, (a, b) 48 h, (c, d) 96 h, (e, f) 144 h, and (g, h) 192 h.

Fig. S8. Optical images of 5% MZ-CPE for ball-milling duration of (a) after 96 h, (b) after 144 h and (c) after 192 h.

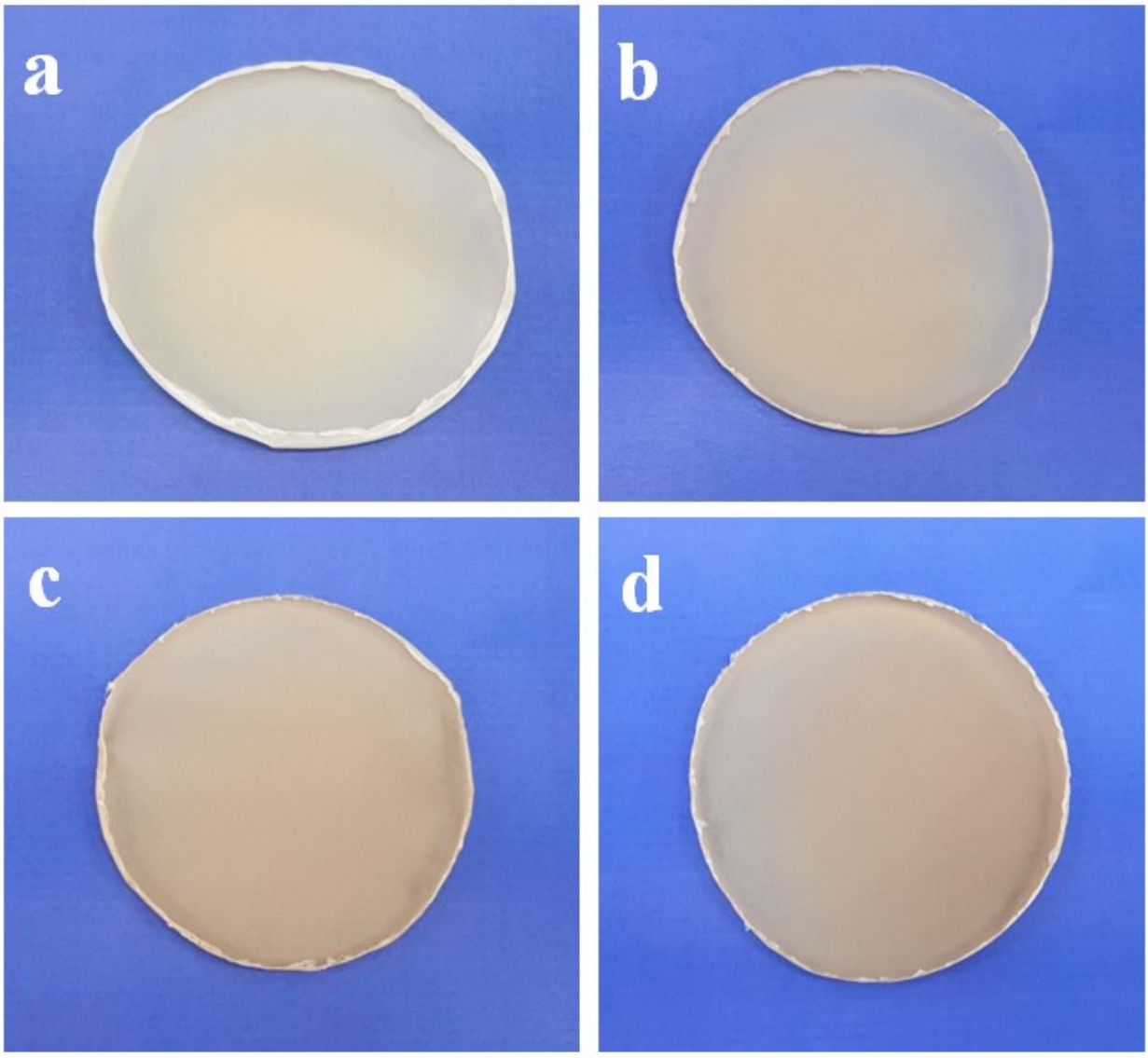

Fig. S9. Optical images of MZ-CPE films for various contents of M-SSZ-13 after 48 h of ball-milling (a) 5% MZ-CPE, (b) 10% MZ-CPE, (c) 15% MZ-CPE and (d) 20% MZ-CPE.

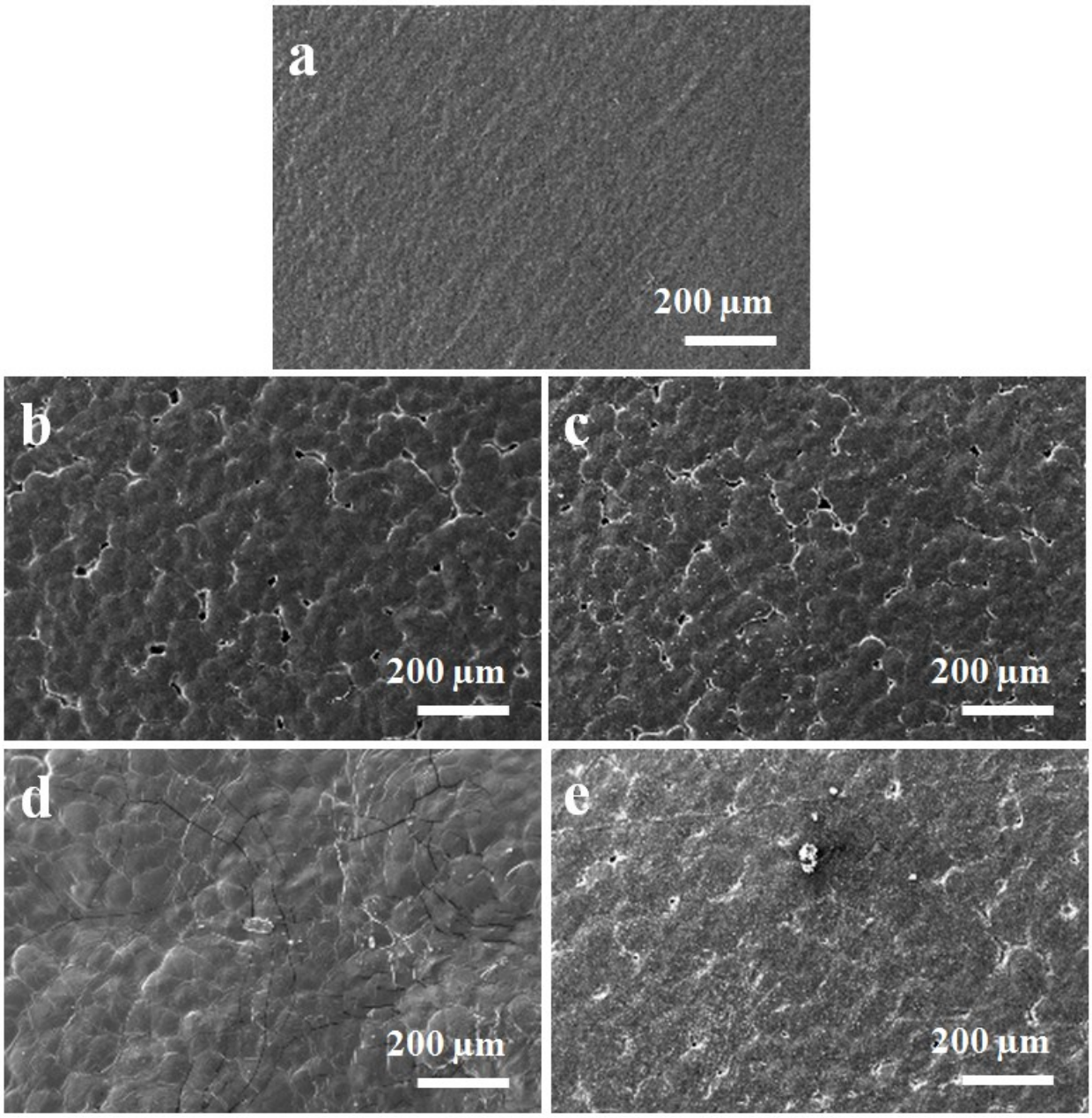

Fig. S10. SEM images of (a) SPE, (b) 5% MZ-CPEs, (c) 10% MZ-CPE, (d) 15% MZ-CPE, and (e) 20% MZ-CPE solid electrolytes.

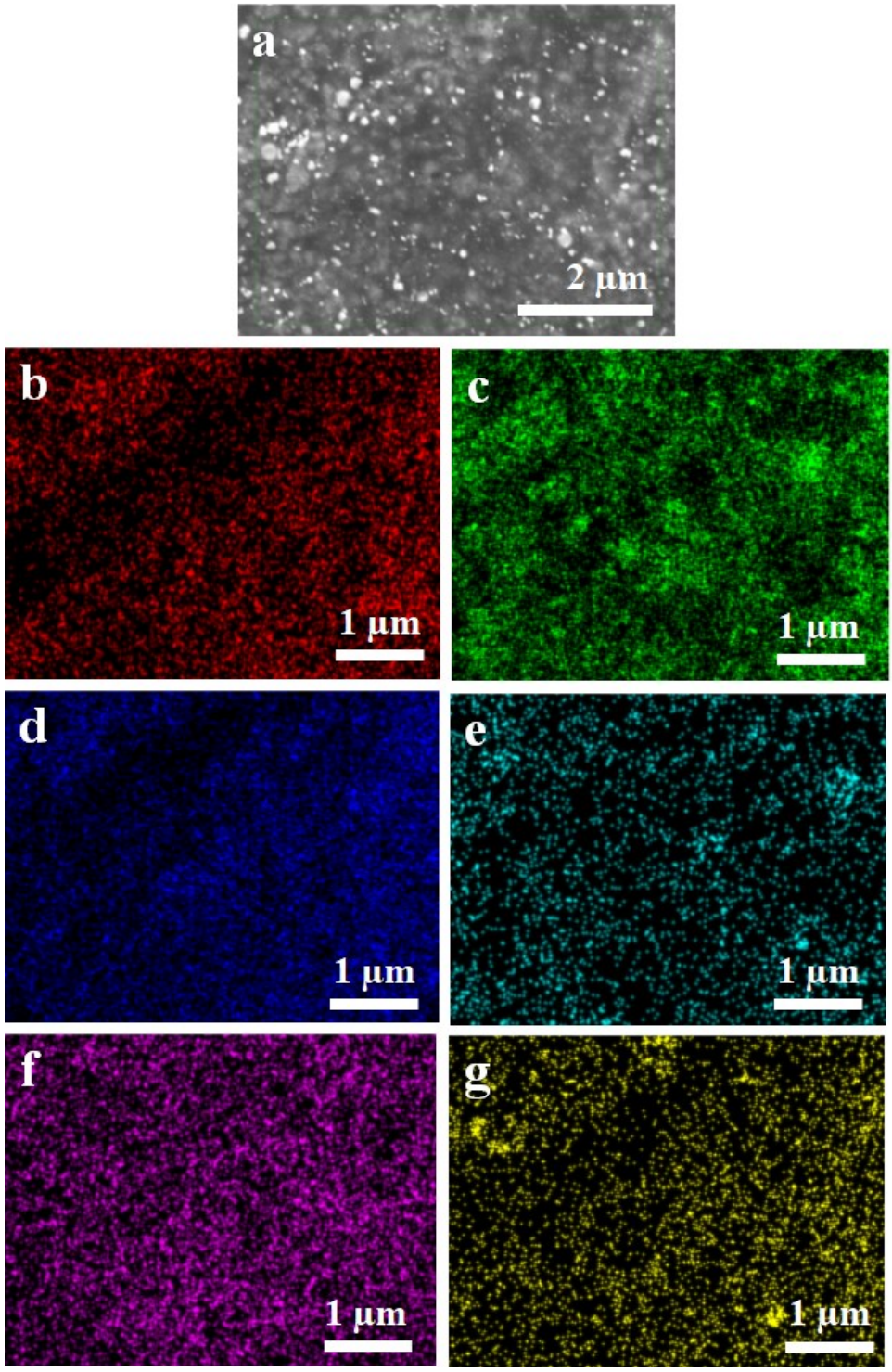

Fig. S11. FE-SEM image of (a) 5% MZ-CPE, and EDX mapping of 5% MZ-CPE for (b) C, (c) Si, (d) O, (e) Al, (f) S, and (g) F elements.

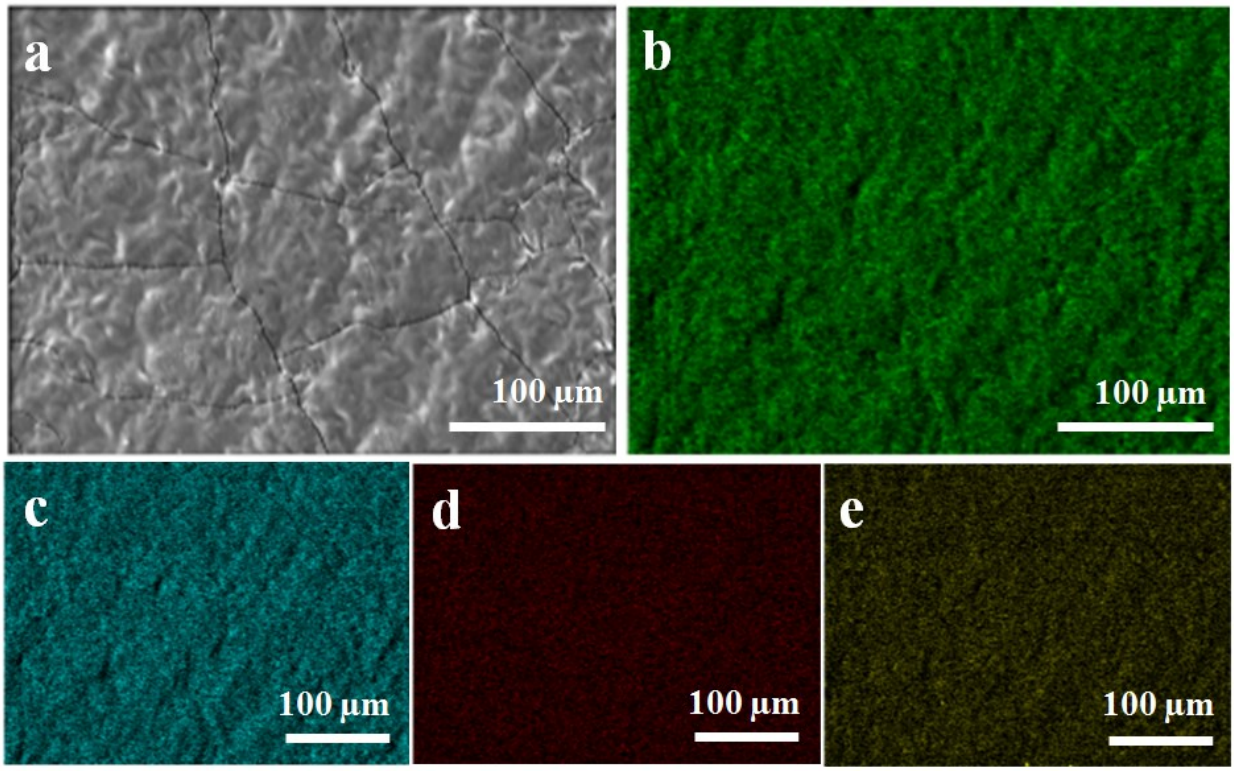

Fig. S12. SEM image (a) SPE, and EDX mapping of SPE for (b) C, (c) O, (d) S, and (e) F elements.

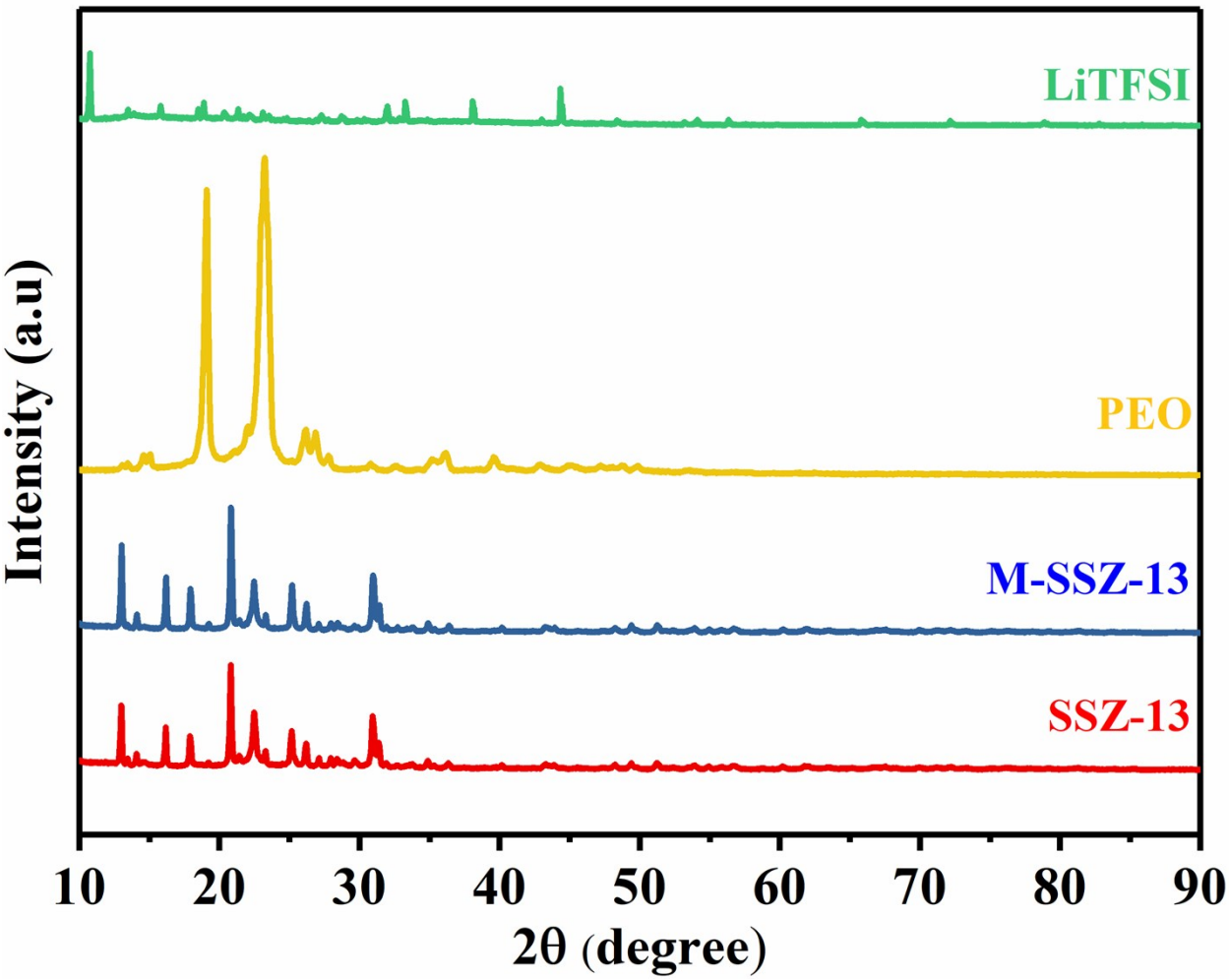

Fig. S13. XRD patterns of SSZ-13, M-SSZ-13, PEO and LiTFSI from 10^0 to 90^0.

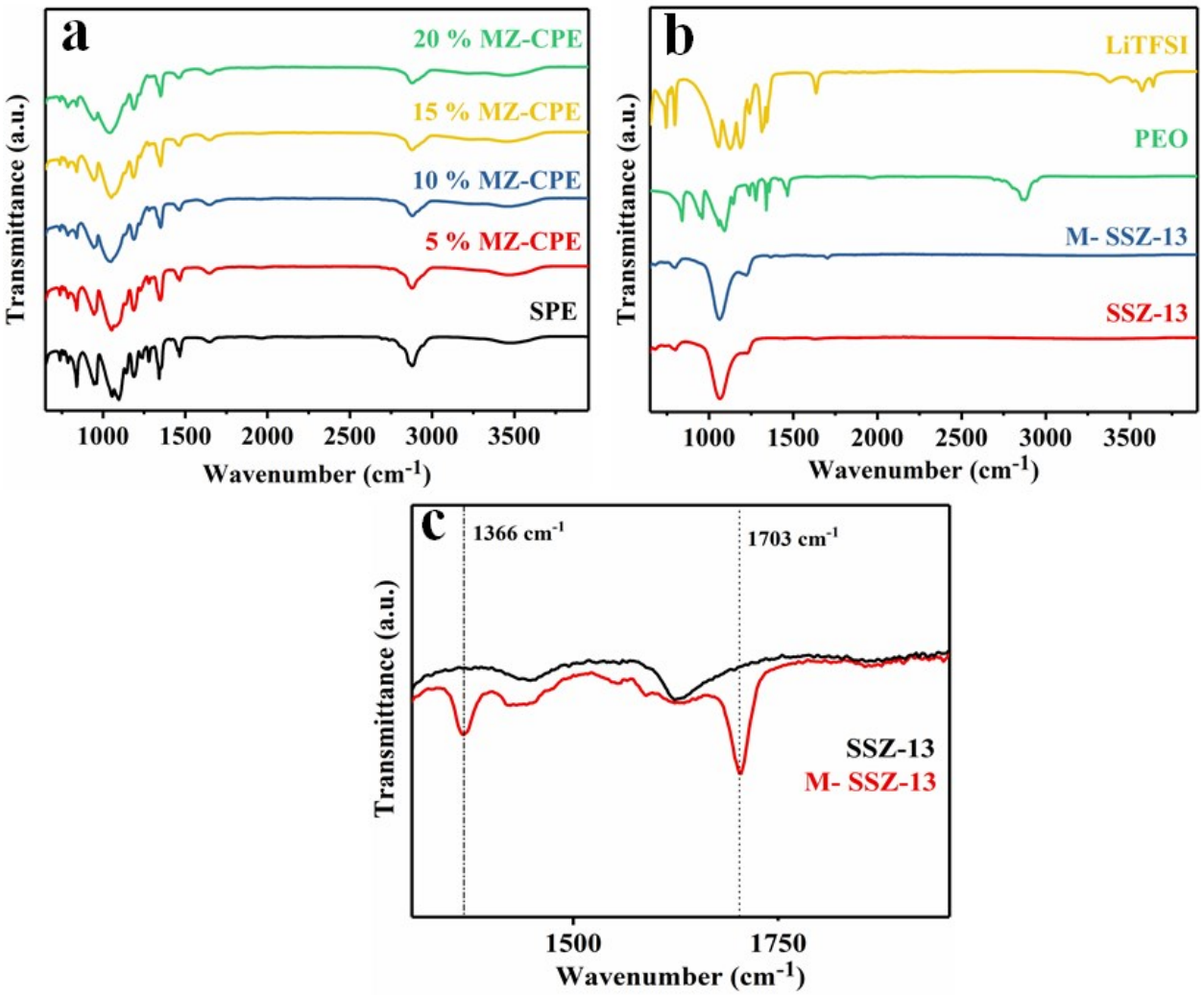

Fig. S14. (a) FTIR spectra of SPE, 5% MZ-CPE, 10% MZ-CPE, 15% MZ-CPE and 20% MZ-CPE between 650–3900 cm^{-1}, (b) FTIR spectra of SSZ-13, M-SSZ-13, PEO and LiTFSI between 650–3900 cm^{-1}, and (c) Magnified FTIR spectra of SSZ-13 and M-SSZ-13 in the range of 1303–1959 cm^{-1}.

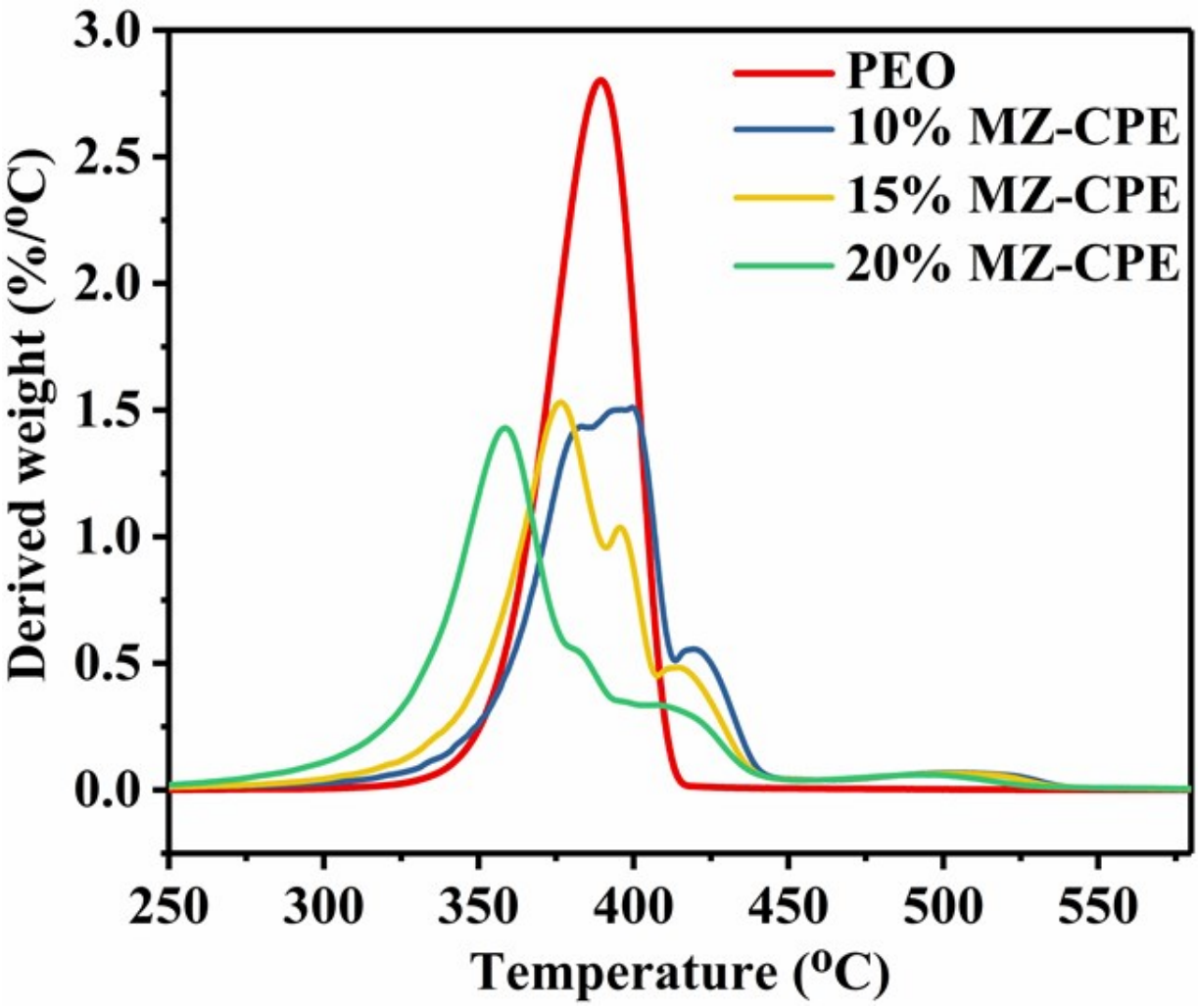

Fig. S15. Derived weight vs. temperature curves for PEO, 10% MZ-CPE, 15% MZ-CPE and 20% MZ-CPE in the temperature range of 250 - 600 ℃.

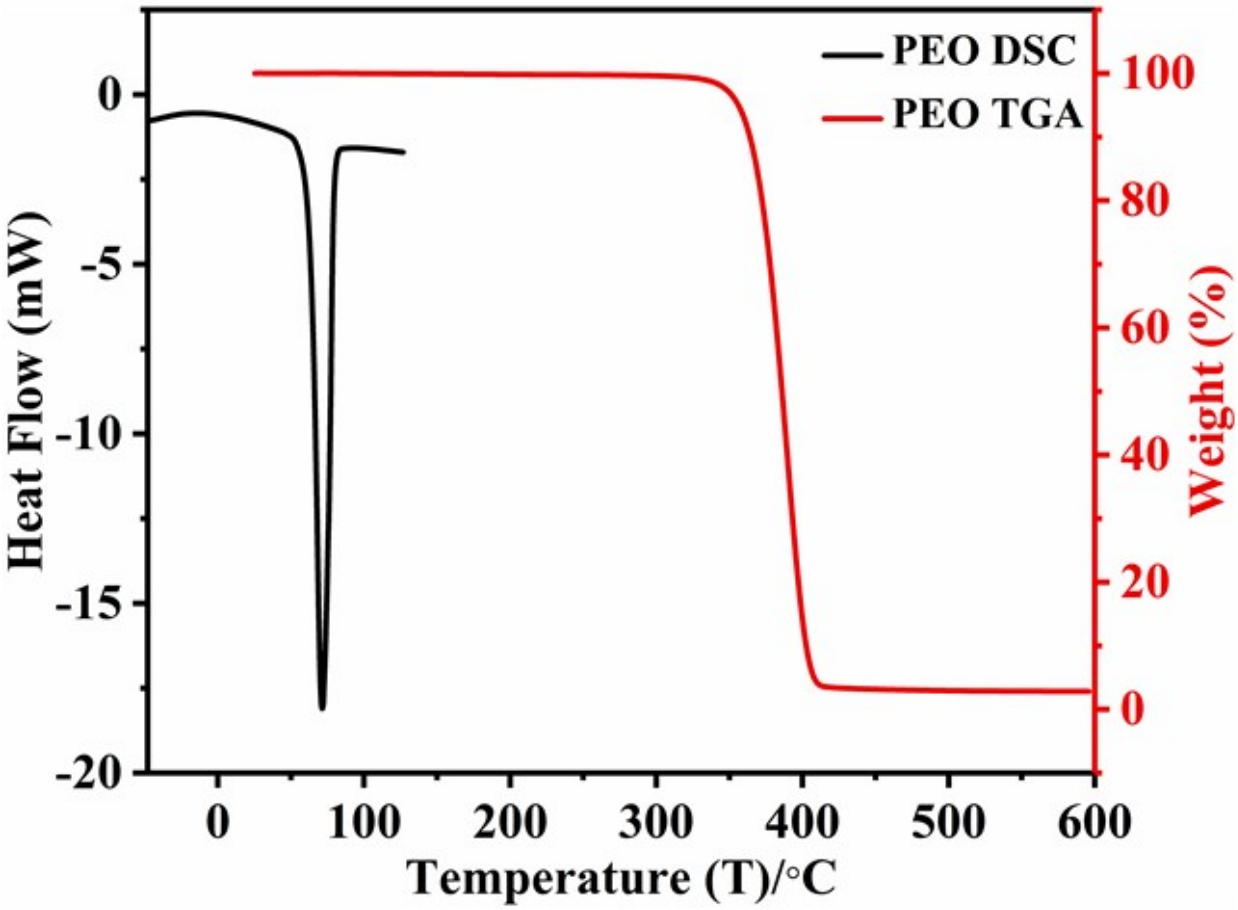

Fig. S16. DSC and TGA curves of PEO in the temperature ranges of -50 ℃ – 150 ℃ and 25 – 600 ℃, respectively. All analysis is made under the flow of N_2 along with heating ramp-rate of 10 ℃/min.

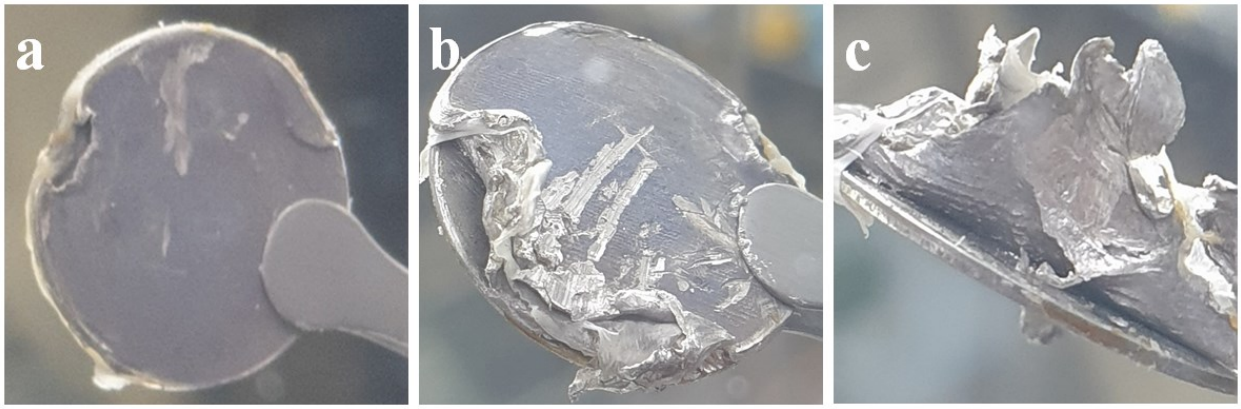

Fig. S17. (a-c) Optical images of symmetrical coin cell [Li|5% MZ-CPE|Li] after the activation @70 ℃ for 2 h. The 5% MZ-CPE very strongly attached with Li-metal.

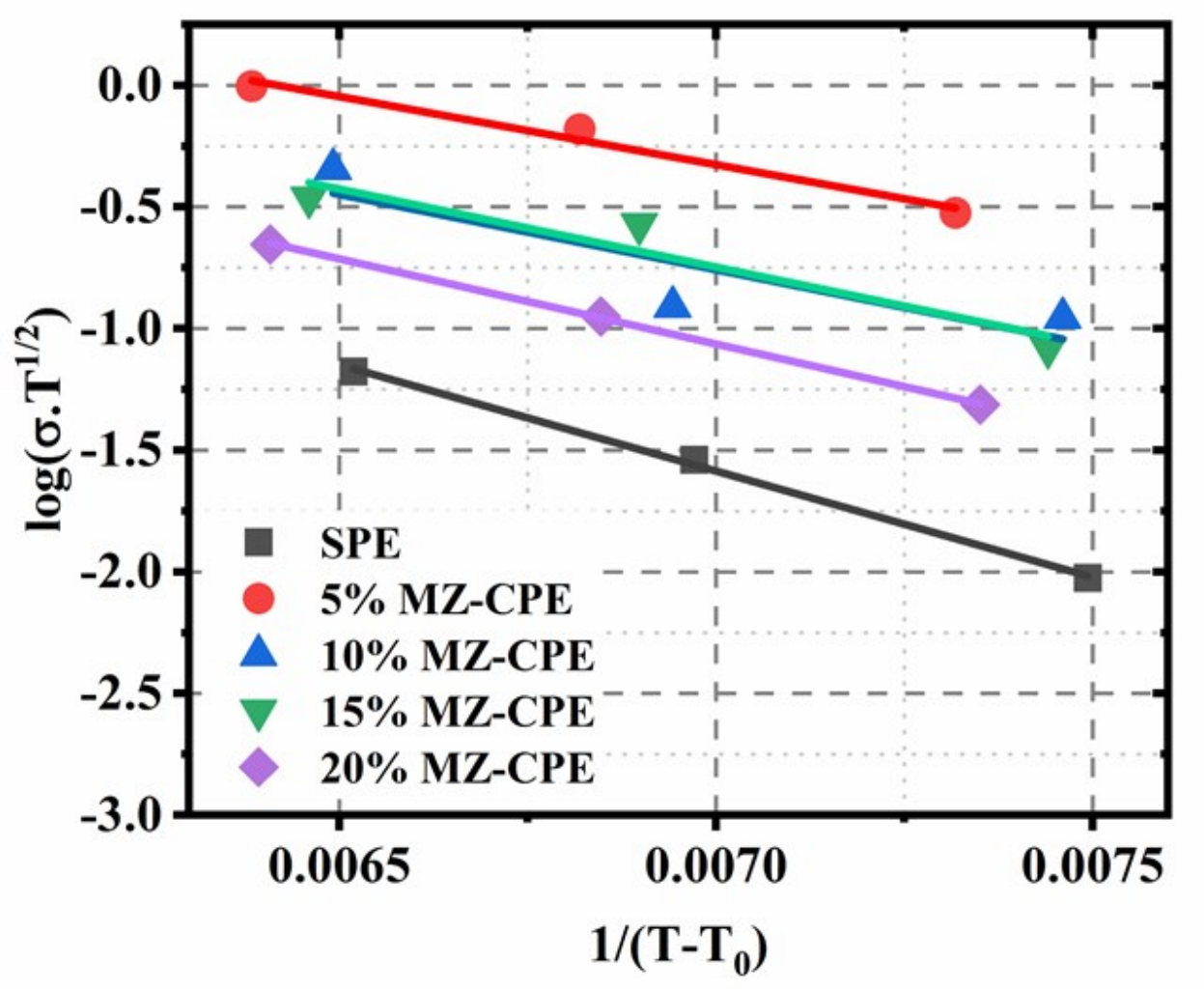

Fig. S18. VTF fitting results [between $log\left(\sigma.T^{1/2}\right)$ vs. $\frac{1}{(T-T_0)}$] for determination of the activation energy of SPE and MZ-CPEs (5%, 10%, 15%, and 20%).

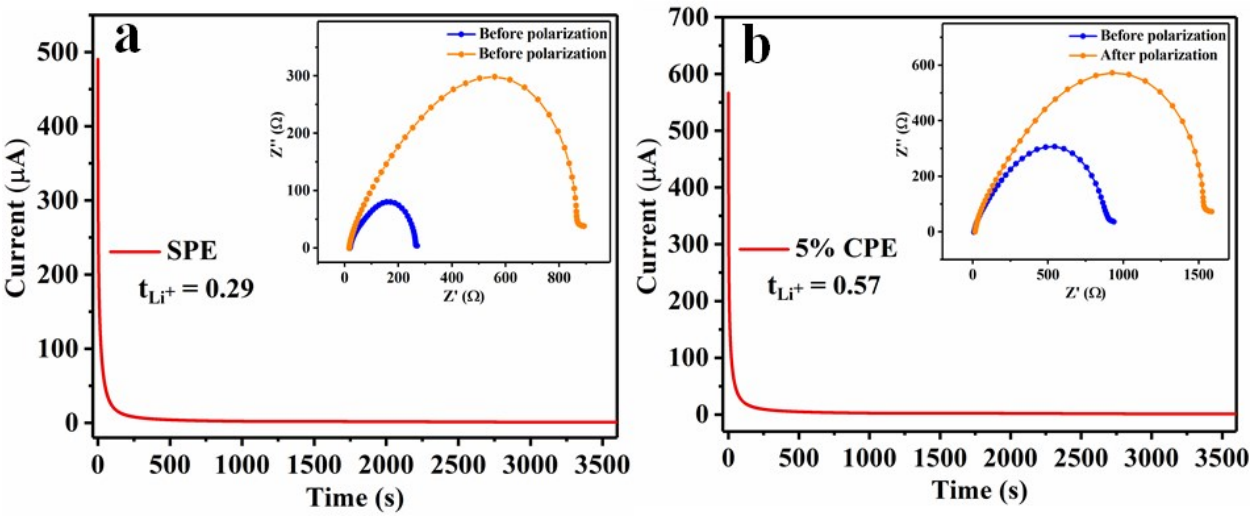

Fig. S19. Current-time profile of (a) SPE for Li symmetric batteries [Li|SPE|Li] @60 ℃ (Inset: Nyquist plots before and after polarization) and (b) 5% CPE for Li symmetric batteries [Li|5% CPE|Li] @60 ℃ (Inset: Nyquist plots before and after polarization).

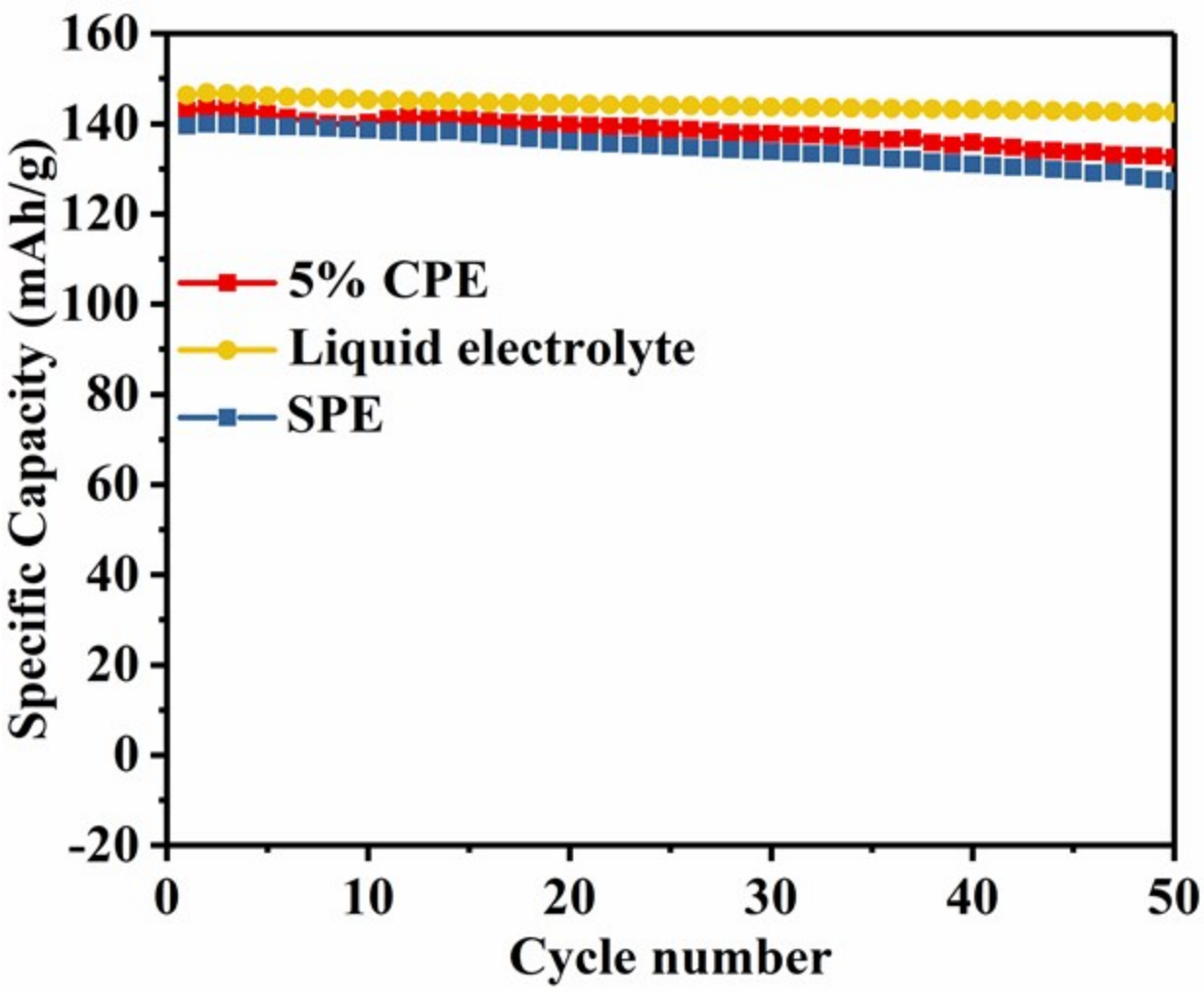

Fig. S20. Comparison of cycling performance of 5% CPE with the cell structure of [Li|5% CPE|LFP] (@60 ℃), liquid electrolyte with cell structure of [Li|liquid electrolyte|LFP] (@30 ℃) and SPE with cell structure of [Li|SPE|LFP] (@60 ℃) at the discharge current density of 0.1 C.

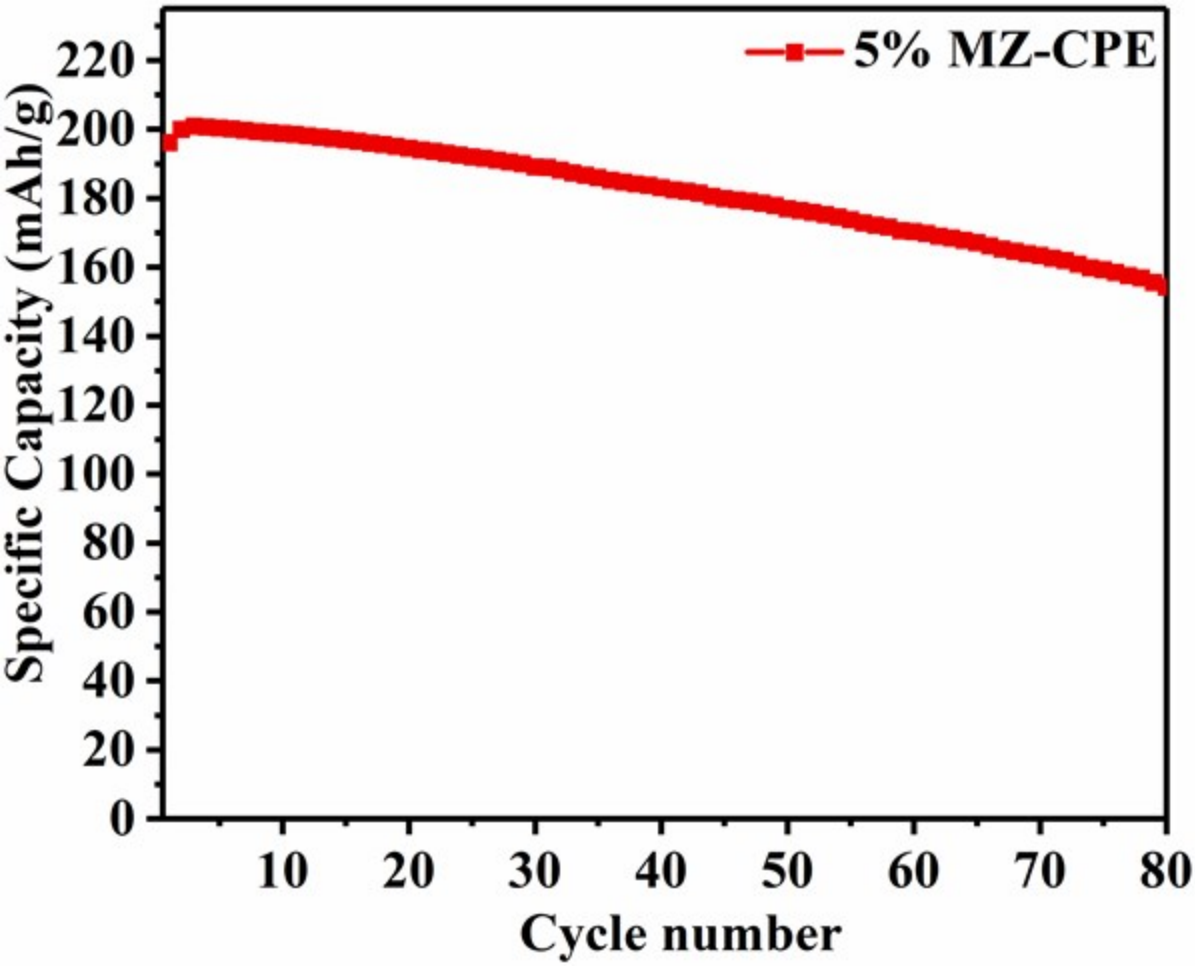

Fig. S21. Cycling performance of 5% MZ-CPE with cell structure of [Li|5% MZ-CPE|NCA] at the discharge current density of 0.1 C (@60 ℃).

References

[1] Shalu, V. K. Singh and R. K. Singh, *J. Mater. Chem. C*, 2015, **3**, 7305–7318.

[2] S. K. Chaurasia, A. L. Saroj, Shalu, V. K. Singh, A. K. Tripathi, A. K. Gupta, Y. L. Verma and R. K. Singh, AIP Adv, 2015, **3,** 077178.

[3] D. M. Pesko, Y. Jung, A. L. Hasan, M. A. Webb, G. W. Coates, T. F. Miller and N. P. Balsara, Solid State Ionics, 2016, 289, 118–124.

[4] C. Zhang, Y. Lin and J. Liu, J. Mater. Chem. A, 2015, **3,** 10760–10766.

[5] W. Zhou, H. Gao and J. B. Goodenough, Adv. Energy Mater, 2016, **6,** 1501802–1501810.

[6] D. Lin, W. Liu, Y. Liu, H. R. Lee, P. C. Hsu, K. Liu and Y. Cui, Nano Lett., 2016, **16,** 459–465.

[7] J. Zhang, N. Zhao, M. Zhang, Y. Li, P. K. Chu, X. Guo, Z. Di, X. Wang and H. Li, Nano Energy, 2016, **28,** 447–454.

[8] O. Sheng, C. Jin, J. Luo, H. Yuan, C. Fang, H. Huang, Y. Gan, J. Zhang, Y. Xia, C. Liang, W. Zhang and X. Tao, J. Mater. Chem. A, 2017, **5,** 12934–12942.

[9] W. Li, S. Zhang, B. Wang, S. Gu, D. Xu, J. Wang, C. Chen and Z. Wen, ACS Appl. Mater. Interfaces, 2018, **10,** 23874–23882.

[10] W. Zha, F. Chen, D. Yang, Q. Shen and L. Zhang, J. Power Sources, 2018, **397,** 87–94.

[11] H. Yuan, J. Luan, Z. Yang, J. Zhang, Y. Wu, Z. Lu and H. Liu, ACS Appl. Mater. Interfaces, 2020, **12,** 7249–7256.